


 Cite this: *RSC Adv.*, 2021, **11**, 33245

The radical scavenging activity of muriolide in physiological environments: mechanistic and kinetic insights into double processes†

 Nguyen Thi Hoa,^a Le Thi Ngoc Van^b and Quan V. Vo  ^{*a}

Muriolide (**MO**) is a natural lactone that was isolated from *Ranunculus muricatus*. This compound exhibited good antioxidant activity in some experiments; however, the radical scavenging activity of **MO** in physiological environments has not been studied yet. In this study, the reaction between hydroperoxy radical and **MO** was investigated in physiological environments by using density functional theory (DFT) calculations. It was found that **MO** exhibits excellent antiradical activity in water at physiological pH ($k = 1.05 \times 10^8 \text{ M}^{-1} \text{ s}^{-1}$) by the single electron transfer mechanism of the anion state. However, the activity in lipid media is moderate with $k = 2.54 \times 10^4 \text{ M}^{-1} \text{ s}^{-1}$ and is defined by the formal hydrogen transfer pathway. The antiradical reactions can occur in double processes; however, the first reaction may define the HOO^\cdot radical scavenging activity of **MO**. Compared with typical natural antioxidants, the antiradical activity of **MO** against HOO^\cdot radicals is slightly lower than Trolox in pentyl ethanoate. However, the activity of **MO** is approximately 808 times faster than that of the reference in aqueous solution. Thus, the data suggest that **MO** is a promising natural radical scavenger in the physiological environment.

 Received 3rd September 2021
 Accepted 5th October 2021

 DOI: 10.1039/d1ra06632c
rsc.li/rsc-advances

1. Introduction

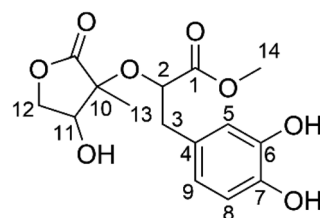
Ranunculus muricatus, which belongs to the genus *Ranunculus* (Ranunculaceae), is known as spiny fruit buttercup in Asia, Australia, South America, and Europe.¹ The plant has been used as a traditional drug to treat urinary infections, jaundice, diarrhea, dysentery, eczema, leprosy, and ringworm infection.^{2–4} *R. muricatus* is also used as a remedy for coughs and asthma and a deworming agent for all types of livestock.^{5,6} Studies showed that *R. muricatus* exhibited cytotoxic, antibacterial, antifungal, and particularly antioxidant properties.^{7,8} The antioxidant activity of *R. muricatus* may be related to phenolic compounds such as flavonoids, flavonoid glycosides, and lactones found in the plant.^{7,9,10}

Muriolide (**MO**, Fig. 1) is a natural lactone that has been isolated from *Ranunculus muricatus*.⁹ This compound exhibited good antioxidant activity against the DPPH radical scavenging activity ($\text{IC}_{50} = 56.9 \mu\text{M}$) and lipoxygenase enzyme testing ($\text{IC}_{50} = 68.3 \mu\text{M}$). Thus the radical scavenging activity of **MO**, particularly in the physiological systems, needs to be investigated; however, this issue has not been mentioned yet. Previous studies have shown that the computational method is one of the most convenient means of examining the relationship between

structures and biological activity in the development of new medicines, such as antioxidants with increased activities.^{11–15} Therefore, in this study, the antiradical activity of **MO** was thoroughly evaluated in double processes by using quantum calculations. In addition, the effects of solvents and molecule structure on the activity were also considered.

2. Computational details

Calculations were carried out with the Gaussian 09 suite of programs¹⁶ by using the M06-2X/6-311++G(d,p) method.¹⁷ The M06-2X functional is one of the most reliable methods to study thermodynamics and the kinetics of radical reactions,^{18–20} and widely used to evaluate the antiradical scavenging activity in solvents (water for polar media and pentyl ethanoate for lipid environments)^{15,21} with low errors compared to experimental


 Muriolide (**MO**)

^aThe University of Danang – University of Technology and Education, Danang 550000, Vietnam. E-mail: vvquan@ute.udn.vn

^bDuy Tan University, Danang 550000, Vietnam

† Electronic supplementary information (ESI) available. See DOI: [10.1039/d1ra06632c](https://doi.org/10.1039/d1ra06632c)

 Fig. 1 Molecular structure of muriolide (**MO**).

data ($k_{\text{calc}}/k_{\text{exp}}$ ratio = 1–2.9).^{21–25} The kinetic calculations were performed following the quantum mechanics-based test for the overall free radical scavenging activity (QM-ORSA) protocol,^{12,21} with the SMD method for solvent effects,²⁶ by the Eyringpy code.^{24,27} All of the species have been optimized directly in the specific environments, *i.e.* gas phase, pentyl ethanoate and water. The rate constant was calculated by using the conventional transition state theory (TST) and 1 M standard state at 298.15 K.^{24,25,27–32}

$$k = \sigma \kappa \frac{k_B T}{h} e^{-(\Delta G^\ddagger)/RT} \quad (1)$$

where σ is the reaction symmetry number,^{33,34} κ contains the tunneling corrections calculated using the Eckart barrier,³⁵ k_B is the Boltzmann constant, h is the Planck constant, ΔG^\ddagger is the Gibbs free energy of activation. The Marcus Theory was used to estimate the reaction barriers of single electron transfer (SET) reactions.^{36–38} The free energy of reaction ΔG^\ddagger for the SET pathway was computed following the eqn (2) and (3).

$$\Delta G_{\text{SET}}^\ddagger = \frac{\lambda}{4} \left(1 + \frac{\Delta G_{\text{SET}}^0}{\lambda} \right)^2 \quad (2)$$

$$\lambda \approx \Delta E_{\text{SET}} - \Delta G_{\text{SET}}^0 \quad (3)$$

where ΔG_{SET} is the Gibbs energy of reaction, ΔE_{SET} is the non-adiabatic energy difference between reactants and vertical products for SET.^{39,40}

For rate constants that were close to the diffusion limit a correction was applied to yield realistic results.²¹ The apparent rate constants (k_{app}) were calculated following the Collins–Kimball theory in the solvents at 298.15 K;⁴¹ the steady-state Smoluchowski rate constant (k_D) for an irreversible

bimolecular diffusion-controlled reaction was calculated following the literature as corrodng to eqn (4) and (5).^{21,42}

$$k_{\text{app}} = \frac{k_{\text{TST}} k_D}{k_{\text{TST}} + k_D} \quad (4)$$

$$k_D = 4\pi R_{\text{AB}} D_{\text{AB}} N_A \quad (5)$$

where R_{AB} is the reaction distance, N_A is the Avogadro constant, and $D_{\text{AB}} = D_A + D_B$ (D_{AB} is the mutual diffusion coefficient of the reactants A and B),^{41,43} where D_A or D_B is estimated using the Stokes–Einstein formulation (6).^{44,45}

$$D_{\text{A or B}} = \frac{k_B T}{6\pi\eta a_{\text{A or B}}} \quad (6)$$

η is the viscosity of the solvents (*i.e.* $\eta(\text{H}_2\text{O}) = 8.91 \times 10^{-4}$ Pa s, $\eta(\text{pentyl ethanoate}) = 8.62 \times 10^{-4}$ Pa s) and a is the radius of the solute that was obtained in Gaussian calculations.

The solvent cage effects were included following the corrections proposed by Okuno,⁴⁶ adjusted with the free volume theory according to the Benson correction^{21,47–49} to reduce over-penalizing entropy losses in solution. All transition states were characterized by the existence of only one single imaginary frequency. Intrinsic coordinate calculations (IRCs) were performed to ensure that each transition state (TS) is connected correctly with the pre-complex (RC) and post-complex (PC).

3. Results and discussion

3.1 The gas phase evaluation

Study of the structure of the MO showed that the molecule can adopt multiple conformational structures. Thus, as an initial step, the possibility of MO conformers was examined⁵⁰ and then the M06-2X/6-311++G(d,p) method was used to analyze the six

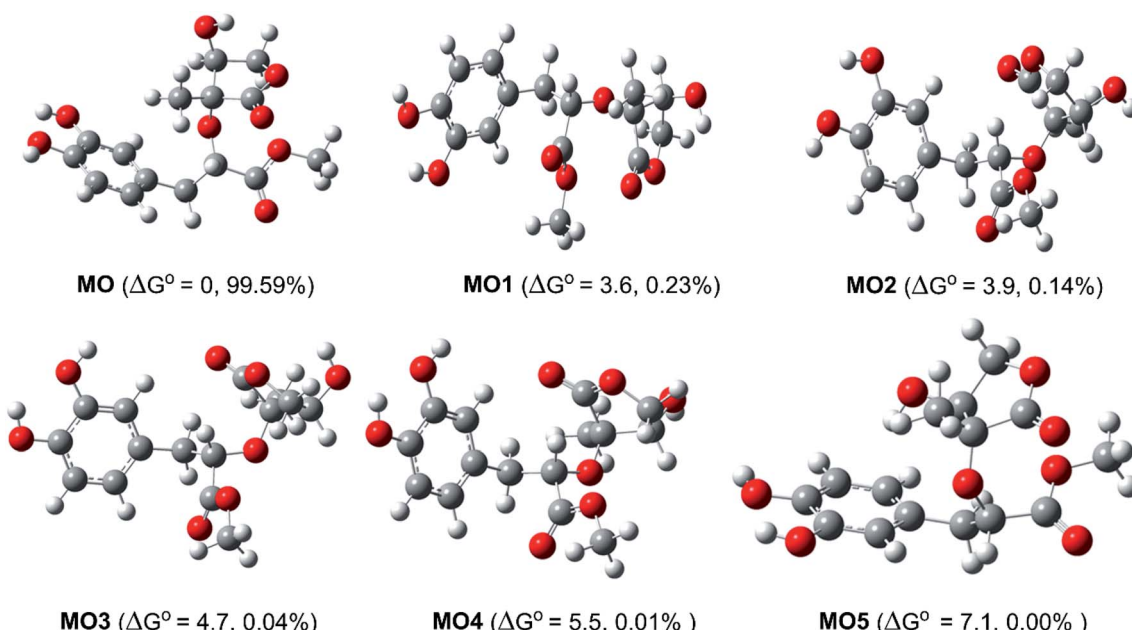


Fig. 2 The typical MO conformers and the relative free energy ΔG^\ddagger (compared with MO, kcal mol^{-1}).



Table 1 Calculated thermodynamic parameters (kcal mol⁻¹) of the **MO** + HOO[·] via FHT, SP and SET reactions

Positions	FHT		SP		SET	
	BDE	ΔG°	PA	ΔG°	IE	ΔG°
C2-H	88.4	3.6			185.0	162.1
C3-H	93.0	7.6				
O6-H	79.6	-5.4	334.6	183.5		
O7-H	79.0	-6.0	332.2	181.1		
O11-H	104.0	18.4	353.8	201.9		
C11-H	98.0	11.4				
C12-H	98.1	11.8				

Table 2 Calculated ΔG[‡] (kcal mol⁻¹), tunneling corrections (κ), *k*_{Eck} (M⁻¹ s⁻¹) and branching ratios (*Γ*, %) for the HOO[·] + **MO** reaction

Positions	ΔG [‡]	κ	<i>k</i> _{Eck}	Γ
O6-H	12.0	169.0	1.63 × 10 ⁶	37.5
O7-H	11.3	77.7	2.71 × 10 ⁶	62.5
<i>k</i> _{overall}			4.34 × 10 ⁶	

lowest electronic energy conformers (Fig. 2). It was found that, the lowest ΔG° value was observed at **MO**, those for **MO1**–**MO5** were higher than that of **MO** about 3.6–7.1 kcal mol⁻¹. With the Maxwell–Boltzmann distribution,^{51,52} it was found that **MO** is the dominant conformer (99.59%) in the relative tautomer populations, and this conformer has therefore been used in further studies.

The radical scavenging activity of **MO** was evaluated against HOO[·] radical. This radical species is the simplest of the biologically most important of the ROO[·], *i.e.* peroxy radicals, and effective scavenging of these is sufficient to reduce oxidative stress in biological systems.⁵³ The HOO[·] radical, which is moderately reactive and one of the main antioxidant objectives,⁵⁴ has been widely used as a reference radical for modeling antioxidant activity in lipid and polar environments.^{12,21,48,55}

To understand how **MO** scavenges free radicals, the antioxidant reactivity of **MO** was first evaluated following the three typical antioxidant mechanisms, including formal hydrogen transfer (FHT), sequential proton loss electron transfer (SPLET), and single electron transfer proton transfer (SETPT).¹¹ Those are

defined by the thermochemical parameters (bond dissociation enthalpy (BDE), proton affinity (PA), and ionization energy (IE), respectively). Previous studies showed that the radical adduct formation (RAF) of HOO[·] radical was not favored for the π system of aromatic rings^{48,56–58} such as in **MO** and therefore this mechanism was not considered in this study. Therefore, the thermodynamic parameters in the gas phase of **MO** were computed and results are presented in Table 1.

The lowest BDE values are presented at the phenolic groups, including O6(O7)-H bonds with BDE = 79.6 and 79.0 kcal mol⁻¹, respectively. The BDE of the alcohol group (O11-H) is highest at 104.0 kcal mol⁻¹, and this is about ~6 and 15.6 kcal mol⁻¹ higher than those of the C11(12)-H bonds and C2-H bond, respectively. Calculated thermodynamic parameters in studied solvents (Table S1, ESI†) indicated that the lowest BDE values were also obtained at the O6(7)-H bonds (BDE(O6(7)-H) = 79.7, 79.0 and 82.6, 82.0 in pentyl ethanoate and water, respectively). Thus the results suggest that the O6(O7)-H bonds will define the H-abstraction of **MO** following the FHT mechanism. It is clear from Table 1 that the PA and IE values are much higher than the BDEs. The lowest PA (PA(O7-H) = 332.2 kcal mol⁻¹) and IE values are around 4.21 and 2.34 times greater than the lowest BDE. Thus the radical scavenging of **MO** in the gas phase may be followed the FHT pathway rather than the SETPT and SPLET mechanisms. This result was confirmed by investigating the Gibbs free energies of the reaction between **MO** and HOO[·] radicals (Table 1).^{25,59} The HOO[·] trapping activity of **MO** is spontaneous for FHT at O6(7)-H bonds (ΔG° = -5.4 and -6.0 kcal mol⁻¹, respectively), whereas the other reactions are non-spontaneous with high positive ΔG° values. Based on the calculated data, the **MO** + HOO[·] reaction may only follow the FHT mechanism, and thus this pathway should be investigated in the kinetic study.

In the next step evaluation of the HOO[·] trapping activity of **MO**, the kinetics of the HOO[·] + **MO** reaction following the primary mechanism (FHT at O6(7)-H bonds) in the gas phase were computed according to the (QM-ORSA) protocol,^{12,21} the results are shown in Table 2 and Fig. 3. It was found that **MO** exhibited moderate hydroperoxyl antiradical activity with *k*_{Eck} = 1.63 × 10⁶ and 2.71 × 10⁶ M⁻¹ s⁻¹ for the O6-H and O7-H bonds, respectively. These reactions contribute about 37.5 and 62.5% in the overall rate constant (*k*_{overall} = 4.34 × 10⁶ M⁻¹ s⁻¹). However, the *k*_{overall} of the HOO[·] + **MO** reaction in the gas phase is ~4.3 times lower than that of Trolox (*k* = 1.87 × 10⁷ M⁻¹

Table 3 Calculated ΔG[‡] (kcal mol⁻¹) and rate constants (*k*_{app}, *k*_f, and *k*_{overall} M⁻¹ s⁻¹) at 298.15 K, in the first process of **MO** + HOO[·] reaction

Mechanisms	Pentyl ethanoate				Water					
	ΔG [‡]	κ	<i>k</i> _{app}	Γ	ΔG [‡]	κ	<i>k</i> _{app}	<i>f</i>	<i>k</i> _f	Γ
SET	MO –O7 ⁻				4.3	16.3 ^a	2.70 × 10 ⁹	0.039	1.05 × 10 ⁸	100.0
FHT	O6-H	15.3	175.3	6.40 × 10 ³	25.2	16.1	932.1	0.961	8.17 × 10 ³	0.0
	O7-H	14.2	79.5	1.90 × 10 ⁴	74.8	15.0	312.8	0.961	2.02 × 10 ⁴	0.0
<i>k</i> _{overall}			2.54 × 10 ⁴						1.05 × 10 ⁸	

^a The nuclear reorganization energy (*λ*, kcal mol⁻¹); *f* = %Δ⁻/100; *k*_f = *f**k*_{app}; *Γ* = *k*_f × 100/*k*_{overall}.



s^{-1}).⁶⁰ Hence, it appears to suggest that the hydroperoxyl anti-radical activity of **MO** in nonpolar media might be lower than that of Trolox.

3.2 The HOO^\cdot radical trapping activity of **MO** in physiological environments

3.2.1 The first process. In aqueous environments, the radical scavenging activity of acidic species is typically dominated by the activity of the ionic forms.^{18,59} Therefore, the protonation state of **MO** was first evaluated at physiological pH to find the most likely radical scavenging reactions. The thermodynamic section and the calculations for water medium (Table S1, ESI,† (PA(O₆-H) = 43.1 kcal mol⁻¹), PA(O₇-H) = 42.9 kcal mol⁻¹) showed that deprotonation was the easiest at

the O₇-H bond; thus, the pK_a value of **MO** was computed for the O₇-H bond based on the literature^{59,61} and shown in Fig. 4.

The calculated pK_a value was $pK_a = 8.79$. Therefore, in pH = 7.40 aqueous solutions, **MO** exists in two states, including the neutral (HA, 96.1%) and anion (A⁻, 3.9%) states. Hence, these states were used in the kinetic study of the HOO^\cdot trapping activity of **MO** in water at pH = 7.4. The overall rate constant (k_{overall}) of $\text{HOO}^\cdot + \text{MO}$ reaction in the first antiradical process were calculated according to eqn (7) and (8); the results are presented in Table 3 and Fig. 3, while the potential energy surfaces of the $\text{HOO}^\cdot + \text{MO}$ reaction following the FHT pathway is shown in Fig. 5.

In lipid medium:

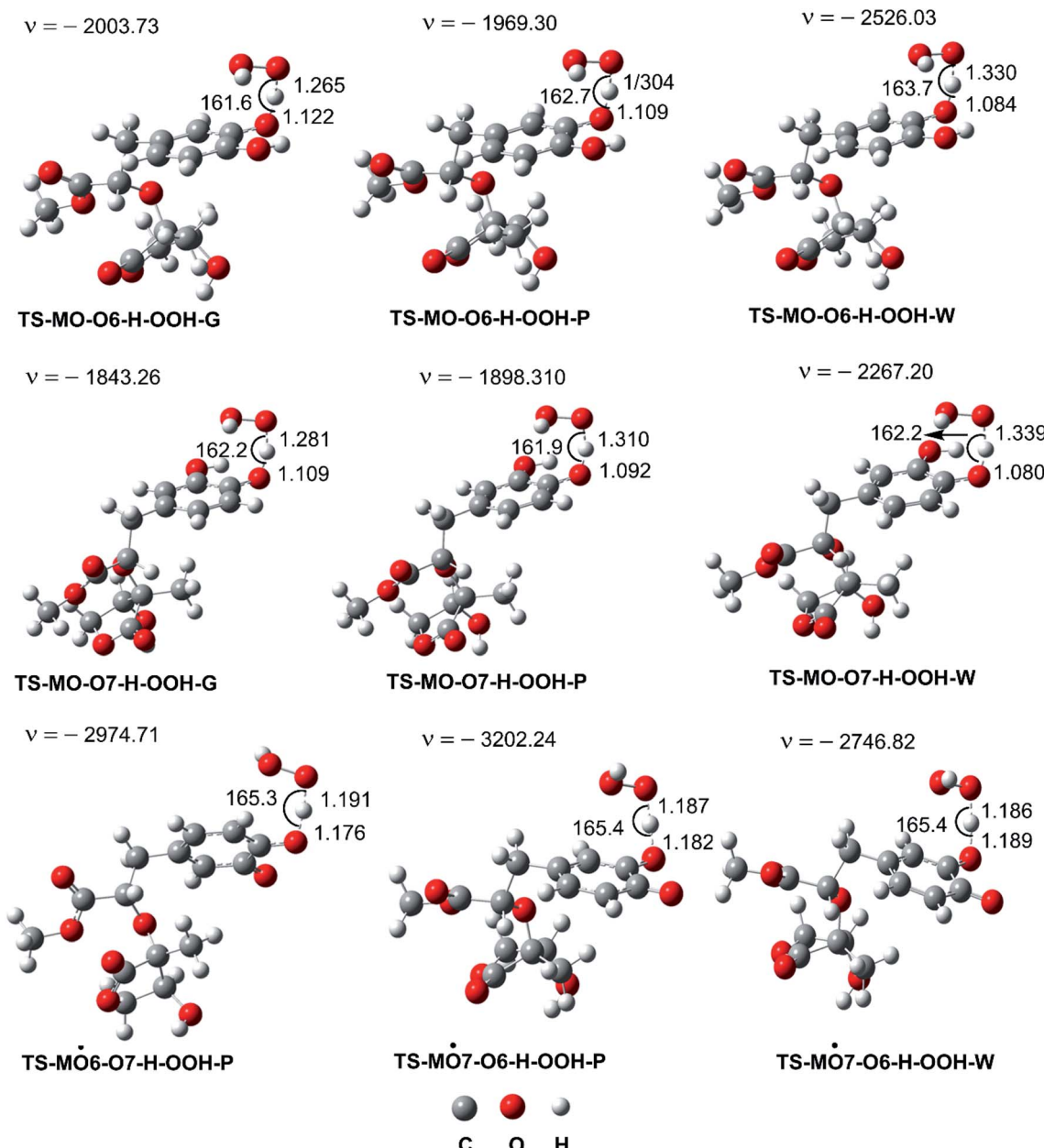


Fig. 3 Optimized geometries of FHT TSs of the $\text{HOO}^\cdot + \text{MO}$ reaction (G: gas phase, W: water, P: pentyl ethanoate).



Table 4 Calculated thermodynamic parameters (kcal mol⁻¹) of the intermediates + HOO[•] via FHT and SET mechanisms in pentyl ethanoate (P) and water (W)

Solvents	Intermediates	Positions	FHT		SET	
			BDE	ΔG°	IE	ΔG°
P	MO-O6'	O7-H	69.2	-16.4	145.9	75.8
	MO-O7'	O6-H	69.9	-16.0	143.9	72.5
W	MO-O7'	O6-H	71.1	-18.8	132.0	26.3

$$k_{\text{overall}} = k_{\text{app}}(\text{FHT(O6-H)-neutral}) + k_{\text{app}}(\text{FHT(O7-H)-neutral}) \quad (7)$$

In the aqueous medium:

$$k_{\text{overall}} = k_f(\text{SET-anion}) + k_f(\text{FHT(O6-H)-neutral}) + k_f(\text{FHT(O7-H)-neutral}) \quad (8)$$

As shown in Fig. 5, in the first antiradical process, the reaction proceeds *via* the RCs that are more stable in terms of energy than the reactants about 3.4–5.8 kcal mol^{−1}. Then, the reaction can proceed to TSs from the RCs (the energy barriers around 12.0–17.0 kcal mol^{−1}) before bottoming the lowest energy points (PCs) and forming the products. The energy barriers for the **MO**–O6–H + HOO[·] reaction in water and pentyl ethanoate are higher (from 0.3 to 2.1 kcal mol^{−1}, respectively) than those of the **MO**–O7–H + HOO[·] reaction. This suggests that the H-abstraction of the O7–H bond against HOO[·] radicals should be faster than that of the O6–H bond.

It is clear from the Table 3 that the hydroperoxyl radical trapping activity of **MO** in pentyl ethanoate is moderate with the

$k_{\text{overall}} = 2.54 \times 10^4 \text{ M}^{-1} \text{ s}^{-1}$ by the H-abstractions of the O6-H ($\Gamma = 25.2\%$) and O7-H bonds ($\Gamma = 74.8\%$). In contrast, **MO** exhibits an excellent HOO[·] trapping activity in the polar medium with the $k_{\text{overall}} = 1.05 \times 10^8 \text{ M}^{-1} \text{ s}^{-1}$. This process was defined by the SET reaction of the anion state (**MO**-O7⁻, $\Gamma \sim 100\%$). The rate constants for the FHT reaction of the O6(7)-H bonds against HOO[·] radical in water are $k_f = 8.17 \times 10^3$ (2.02×10^4) $\text{M}^{-1} \text{ s}^{-1}$, whereas these reactions make negligible contributions ($\sim 0\%$) to the overall HOO[·] antiradical activity of **MO**. However, the reaction at the O7-H bond is faster than that of the O6-H bond in all of the studied media. This is in good agreement with the PES analysis results. Compared with the reference antioxidant Trolox ($k = 1.00 \times 10^5$ and $1.30 \times 10^5 \text{ M}^{-1} \text{ s}^{-1}$ in pentyl ethanoate and water, respectively),⁶⁰ the HOO[·] trapping activity of **MO** is fairly lower in the lipid medium but about 808 times higher in water at physiological pH.

3.2.2 The second process of the radical scavenging. To gain

3.2.2 The second process of the radical scavenging. To gain further insights into the antioxidant of **MO** in the physiological environments, the hydroperoxyl radical scavenging activity of **MO** intermediates (the second antiradical process of **MO**) in pentyl ethanoate and water was investigated. As shown in the first reaction step, the primary intermediates of **MO** + HOO^\cdot reaction in pentyl ethanoate were **MO-O6** $^\cdot$ (25.2%) and **MO-O7** $^\cdot$ (74.8%) radicals, while that for the aqueous solution was **MO-O7** $^\cdot$ (100.0%). Thus these intermediates were used as reactants for the second reaction against HOO^\cdot radicals. The thermodynamic parameters (BDEs, IE) were computed for the most active positions and are shown in Table 4.

As shown in Table 4, the BDE values of the most active positions (O6-H and O7-H bonds) are in the range of 69.2 to 71.1 kcal mol⁻¹, much lower than those of **MO** in the first step (Table 1). At the same time, the calculated IE values of intermediates (**MO**-O6⁺, **MO**-O7⁺) are 132.0–145.9 kcal mol⁻¹.

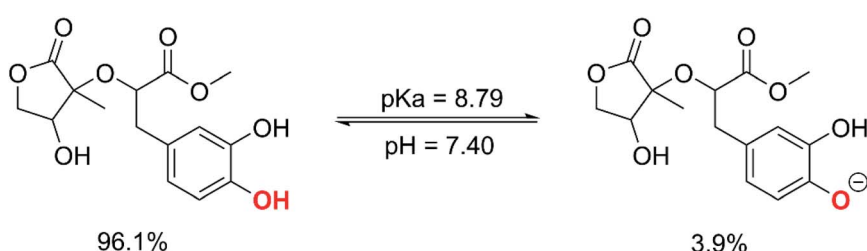


Fig. 4 The deprotonation of MO at pH = 7.4.

Table 5 Calculated ΔG^\ddagger (kcal mol⁻¹) and rate constants ($k_{\text{f},\text{c}}$ and k_{overall} M⁻¹ s⁻¹) at 298.15 K. in the second process of MO + HOO[•] reaction⁶

Mechanisms	Reactions	Pentyl ethanoate		Water	
		$\Delta G^\#$	k_f	$\Delta G^\# (\lambda)$	k_f
SET	MO7[•] + HOO[•]			27.3 (17.7)	5.60×10^{-8}
FHT	MO7[•]-O6-H + HOO[•]	30.5	1.06×10^{-4}	29.1	1.80×10^{-2}
	MO6[•]-O7-H + HOO[•]	30.9	1.20×10^{-6}		
k_{overall}			1.07×10^{-4}		1.80×10^{-2}

^a $k_f = fk_{\text{app}}$; in water $f(\text{intermediate}) = 1.00$; in pentyl ethanoate $f(\text{MO-O7}^{\cdot}) = 0.748$, $f(\text{MO-O6}^{\cdot}) = 0.252$.

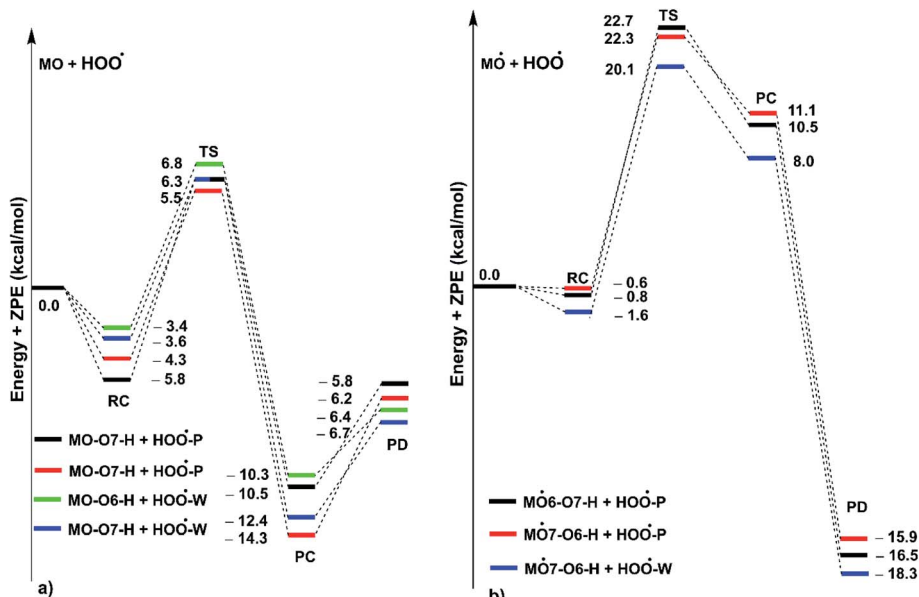


Fig. 5 PES of reactions between MO and HOO[•] in pentyl ethanoate (P) and water (W) in double processes ((a): the first step; (b) the second step; RC: pre-complexes, TS: transition states, PC: post-complexes, PD: products).

however, the SET mechanism is not favored for the intermediates due to the large positive ΔG° ($\Delta G^\circ = 26.3\text{--}75.8\text{ kcal mol}^{-1}$). Thus the HOO[•] radical scavenging activity of intermediates was defined by the FHT pathway ($\Delta G^\circ < 0$, Table 4); thus, these reactions were used for kinetic investigating.

Previous studies also showed that the reaction between antiradical intermediates with radical *i.e.*, HO[•] and HOO[•] most probably proceeds through triplet transition states,^{55,62} and thus, the result was used to evaluate the mechanism and kinetics of the second antiradical reaction of MO. The potential energy surfaces are shown in Fig. 5, whereas the possible mechanisms and kinetic data are presented in Fig. 5 and Table 4, respectively.

As shown in Fig. 5, the reactions of intermediates (MO-O6[•] and MO-O7[•]) and HOO[•] radicals proceed *via* RCs, TSs and PCs, while the PC species are less stable in terms of energy than the reactants. This is in line with previous studies in phenolic compounds.^{55,62} The energy barriers of the reactions are about 20.1–22.7 kcal mol⁻¹, which is much higher than those of the first step (the energy barriers around 12.0–17.0 kcal mol⁻¹, Table 5). The overall rate constants of the intermediates (MO-O6[•] or MO-O7[•]) + HOO[•] reactions in pentyl ethanoate is $1.07 \times 10^{-4}\text{ M}^{-1}\text{ s}^{-1}$, while that for the aqueous solution is $1.80 \times 10^{-2}\text{ M}^{-1}\text{ s}^{-1}$. Thus the HOO[•] radical scavenging activity in the second reaction step of MO following the FHT pathway is about $10^6\text{--}10^8$ times lower than those of the first reaction step (Fig. 6),

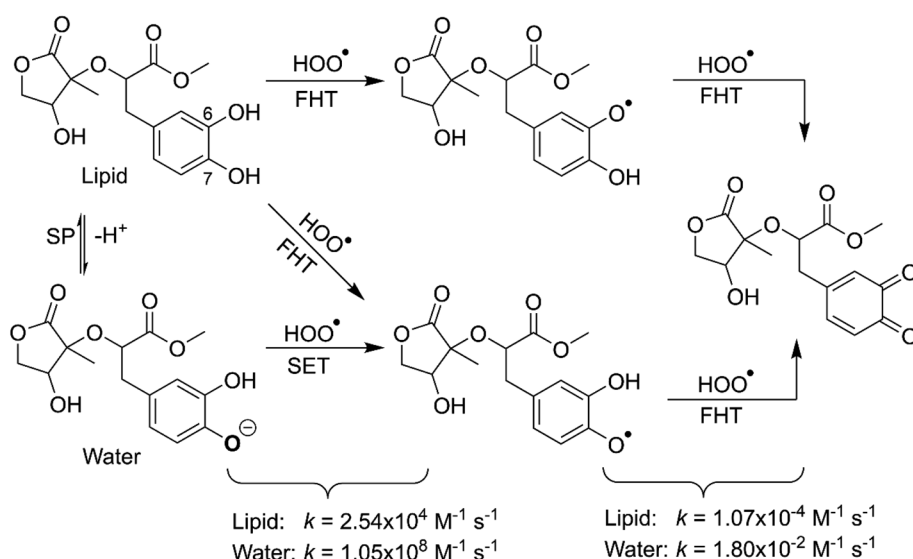


Fig. 6 The possible mechanisms for the HOO[•] + MO reaction in the physiological environment.



despite of the fact that the BDE(O-H) values at the intermediates (BDEs = 69.2–71.1 kcal mol⁻¹, Table 4) are lower than those of **MO** (Table 1) by about 10 kcal mol⁻¹, and the Gibbs free energies for the intermediates (**MO**–O6[•] or **MO**–O7[•]) + HOO[•] reactions are $\Delta G^\circ = -16.0$ to -18.8 kcal mol⁻¹ (Table 4). These results suggest that the HOO[•] radical scavenging of **MO** at the second process is supported by the thermodynamic properties (the low BDE values and $\Delta G^\circ < 0$); however, this reaction hardly occurs due to the low rate constant values. Thus the antiradical activity should be considered in both thermodynamic and kinetic data rather than based on thermodynamic considerations alone. Based on the calculated data, the HOO[•] trapping activity of **MO** in nonpolar and polar environments was mainly defined by the first step.

4. Conclusion

The hydroperoxyl radical scavenging activity of muriolide in the physiological environment has been successfully investigated *in silico*. The result showed that **MO** exhibited moderate activity ($k = 2.54 \times 10^4$ M⁻¹ s⁻¹) in the nonpolar media, whereas the activity was excellent with $k = 1.05 \times 10^8$ M⁻¹ s⁻¹ in water under the physiological pH. The antiradical reactions could occur in two steps; however, the first step reaction defined the HOO[•] radical scavenging activity of **MO**. In nonpolar conditions, the FHT mechanism *via* the O6–H and O7–H bonds determined the antiradical activity, whereas the SET mechanism of the anionic state defined the activity in the polar medium. The HOO[•] + **MO** reaction in pentyl ethanoate is slightly lower than Trolox, but it is approximately 808 times faster than that of the reference in the aqueous solution. Thus, **MO** is an effective radical scavenger in the physiological environment.

Conflicts of interest

There are no conflicts to declare.

Acknowledgements

This research is funded by the Vietnamese Ministry of Education and Training under project number B2021-DNA-16 (Q. V. V.).

References

- 1 B.-L. Wu, H.-L. Zou, F.-M. Qin, H.-Y. Li and G.-X. Zhou, *Molecules*, 2015, **20**, 22445–22453.
- 2 H. Iqbal, Z. Sher and Z. U. Khan, *J. Med. Plants Res.*, 2011, **5**, 2157–2168.
- 3 M. Ullah, M. U. Khan, A. Mahmood, R. N. Malik, M. Hussain, S. M. Wazir, M. Daud and Z. K. Shinwari, *J. Ethnopharmacol.*, 2013, **150**, 918–924.
- 4 M. Umair, M. Altaf and A. M. Abbasi, *PLoS One*, 2017, **12**, e0177912.
- 5 J. Khan, R. Khan and R. Qureshi, *J. Med. Plants Stud.*, 2013, **1**, 1–6.
- 6 H. Sher and M. Alyemeni, *Afr. J. Biotechnol.*, 2011, **10**, 9153–9159.
- 7 F. A. Khan, M. Zahoor and E. Khan, *Pak. J. Pharm. Sci.*, 2016, **29**, 503–510.
- 8 S. Nazir, K. Tahir, R. Naz, Z. Khan, A. Khan, R. Islam and A. U. Rehman, *J. Pharmacol.*, 2014, **8**, 427–431.
- 9 N. Raziq, M. Saeed, M. S. Ali, M. Lateef, M. Shahid, S. Akbar and S. Zafar, *Nat. Prod. Res.*, 2020, 1–7.
- 10 F. Azam, B. A. Chaudhry, H. Ijaz and M. I. Qadir, *Sci. Rep.*, 2019, **9**, 1–6.
- 11 K. U. Ingold and D. A. Pratt, *Chem. Rev.*, 2014, **114**, 9022–9046.
- 12 A. Galano and J. Raúl Alvarez-Idaboy, *Int. J. Quantum Chem.*, 2019, **119**, e25665.
- 13 C. S. Challa, N. K. Katari, V. Nallanchakravarthula, D. Nayakanti, R. Kapavarapu and M. Pal, *J. Mol. Struct.*, 2021, **1245**, 131069.
- 14 G. Dhananjaya, A. D. Rao, K. A. Hossain, V. R. Anna and M. Pal, *Tetrahedron Lett.*, 2020, **61**, 151972.
- 15 Q. V. Vo, T. V. Gon, M. V. Bay and A. Mechler, *J. Phys. Chem. B*, 2019, **123**, 10672–10679.
- 16 M. J. Frisch, G. W. Trucks, H. B. Schlegel, G. E. Scuseria, M. A. Robb, J. R. Cheeseman, G. Scalmani, V. Barone, B. Mennucci, G. A. Petersson, H. Nakatsuji, M. Caricato, X. Li, A. F. I. H. P. Hratchian, J. Bloino, G. Zheng, M. H. J. L. Sonnenberg, M. Ehara, K. Toyota, J. H. R. Fukuda, M. Ishida, T. Nakajima, Y. Honda, H. N. O. Kitao, T. Vreven, J. A. Montgomery, Jr, F. O. J. E. Peralta, M. J. Bearpark, J. Heyd, K. N. K. E. N. Brothers, V. N. Staroverov, R. Kobayashi, K. R. J. Normand, A. P. Rendell, J. C. Burant, J. T. S. S. Iyengar, M. Cossi, N. Rega, N. J. Millam, J. E. K. M. Klene, J. B. Cross, V. Bakken, C. Adamo, R. G. J. Jaramillo, R. E. Stratmann, O. Yazyev, R. C. A. J. Austin, C. Pomelli, J. W. Ochterski, K. M. R. L. Martin, V. G. Zakrzewski, G. A. Voth, J. J. D. P. Salvador, S. Dapprich, A. D. Daniels, J. B. F. Ö. Farkas, J. V. Ortiz, J. Cioslowski, and D. J. Fox, *Gaussian 09*, Gaussian, Inc., Wallingford CT, 2009.
- 17 Y. Zhao and D. G. Truhlar, *Theor. Chem. Acc.*, 2008, **120**, 215–241.
- 18 A. Galano and J. R. Alvarez-Idaboy, *J. Comput. Chem.*, 2014, **35**, 2019–2026.
- 19 Y. Zhao and D. G. Truhlar, *J. Phys. Chem. A*, 2008, **112**, 1095–1099.
- 20 M. Carreon-Gonzalez, A. Vivier-Bunge and J. R. Alvarez-Idaboy, *J. Comput. Chem.*, 2019, **40**, 2103–2110.
- 21 A. Galano and J. R. Alvarez-Idaboy, *J. Comput. Chem.*, 2013, **34**, 2430–2445.
- 22 J. R. I. Alvarez-Idaboy and A. Galano, *J. Phys. Chem. B*, 2012, **116**, 9316–9325.
- 23 M. E. Alberto, N. Russo, A. Grand and A. Galano, *Phys. Chem. Chem. Phys.*, 2013, **15**, 4642–4650.
- 24 E. Dzib, J. L. Cabellos, F. Ortiz-Chi, S. Pan, A. Galano and G. Merino, *Int. J. Quantum Chem.*, 2019, **119**, e25686.



25 H. Boulebd, I. Amine Khodja, M. V. Bay, N. T. Hoa, A. Mechler and Q. V. Vo, *J. Phys. Chem. B*, 2020, **124**, 4123–4131.

26 C. P. Kelly, C. J. Cramer and D. G. Truhlar, *J. Chem. Theory Comput.*, 2005, **1**, 1133–1152.

27 E. Dzib, J. L. Cabellos, F. Ortiz-Chi, S. Pan, A. Galano and G. Merino, *Eyringpy 1.0.2*, Cinvestav, Mérida, Yucatán, 2018.

28 M. G. Evans and M. Polanyi, *Trans. Faraday Soc.*, 1935, **31**, 875–894.

29 H. Eyring, *J. Chem. Phys.*, 1935, **3**, 107–115.

30 D. G. Truhlar, W. L. Hase and J. T. Hynes, *J. Phys. Chem.*, 1983, **87**, 2664–2682.

31 T. Furuncuoglu, I. Ugur, I. Degirmenci and V. Aviyente, *Macromolecules*, 2010, **43**, 1823–1835.

32 E. Vélez, J. Quijano, R. Notario, E. Pabón, J. Murillo, J. Leal, E. Zapata and G. Alarcón, *J. Phys. Org. Chem.*, 2009, **22**, 971–977.

33 E. Pollak and P. Pechukas, *J. Am. Chem. Soc.*, 1978, **100**, 2984–2991.

34 A. Fernández-Ramos, B. A. Ellingson, R. Meana-Pañeda, J. M. Marques and D. G. Truhlar, *Theor. Chem. Acc.*, 2007, **118**, 813–826.

35 C. Eckart, *Phys. Rev.*, 1930, **35**, 1303.

36 R. A. Marcus, *Annu. Rev. Phys. Chem.*, 1964, **15**, 155–196.

37 R. A. Marcus, *Rev. Mod. Phys.*, 1993, **65**, 599.

38 Y. Lu, A. Wang, P. Shi, H. Zhang and Z. Li, *PLoS One*, 2015, **10**, e0133259.

39 S. F. Nelsen, S. C. Blackstock and Y. Kim, *J. Am. Chem. Soc.*, 1987, **109**, 677–682.

40 S. F. Nelsen, M. N. Weaver, Y. Luo, J. R. Pladziewicz, L. K. Ausman, T. L. Jentzsch and J. J. O'Konek, *J. Phys. Chem. A*, 2006, **110**, 11665–11676.

41 F. C. Collins and G. E. Kimball, *J. Colloid Sci.*, 1949, **4**, 425–437.

42 M. Von Smoluchowski, *Z. Phys. Chem.*, 1917, **92**, 129–168.

43 D. G. Truhlar, *J. Chem. Educ.*, 1985, **62**, 104.

44 A. Einstein, *Ann. Phys.*, 1905, **17**, 549–560.

45 G. G. Stokes, *Mathematical and Physical Papers*, University Press, Cambridge, 1905.

46 Y. Okuno, *Chem.-Eur. J.*, 1997, **3**, 212–218.

47 S. Benson, *The Foundations of Chemical Kinetics*, Malabar, Florida, 1982.

48 C. Iuga, J. R. Alvarez-Idaboy and A. Vivier-Bunge, *J. Phys. Chem. B*, 2011, **115**, 12234–12246.

49 J. R. Alvarez-Idaboy, L. Reyes and N. Mora-Diez, *Org. Biomol. Chem.*, 2007, **5**, 3682–3689.

50 W. Hehre, J. Yu, P. Klunzinger and L. Lou, *Spartan Software, Wavefunction.Inc.*, Irvine, 2000.

51 A. Galano and J. R. Alvarez-Idaboy, *RSC Adv.*, 2011, **1**, 1763–1771.

52 Q. V. Vo, N. M. Tam, M. Van Bay, N. M. Thong, T. Le Huyen, N. T. Hoa and A. Mechler, *RSC Adv.*, 2020, **10**, 14937–14943.

53 P. Terpinc and H. Abramović, *Food Chem.*, 2010, **121**, 366–371.

54 T. Masuda, K. Yamada, T. Maekawa, Y. Takeda and H. Yamaguchi, *J. Agric. Food Chem.*, 2006, **54**, 6069–6074.

55 D. S. Dimić, D. A. Milenković, E. H. Avdović, D. J. Nakarada, J. M. D. Marković and Z. S. Marković, *Chem. Eng. Sci.*, 2021, 130331.

56 M. Cordova-Gomez, A. Galano and J. R. Alvarez-Idaboy, *RSC Adv.*, 2013, **3**, 20209–20218.

57 C. Iuga, J. R. I. Alvarez-Idaboy and N. Russo, *J. Org. Chem.*, 2012, **77**, 3868–3877.

58 Q. V. Vo, P. C. Nam, M. Van Bay, N. M. Thong and A. Mechler, *RSC Adv.*, 2019, **9**, 42020–42028.

59 H. Boulebd, A. Mechler, N. T. Hoa and Q. V. Vo, *New J. Chem.*, 2020, **44**, 9863–9869.

60 Q. V. Vo, N. M. Thong, T. Le Huyen, P. C. Nam, N. M. Tam, N. T. Hoa and A. Mechler, *RSC Adv.*, 2020, **10**, 20089–20097.

61 A. Galano, A. Pérez-González, R. Castañeda-Arriaga, L. Muñoz-Rugeles, G. Mendoza-Sarmiento, A. Romero-Silva, A. Ibarra-Escutia, A. M. Rebollar-Zepeda, J. R. León-Carmona, M. A. Hernández-Olivares and J. R. Alvarez-Idaboy, *J. Chem. Inf. Model.*, 2016, **56**, 1714–1724.

62 D. A. Milenković, D. S. Dimić, E. H. Avdović, A. D. Amić, J. M. D. Marković and Z. S. Marković, *Chem. Eng. Sci.*, 2020, **395**, 124971.

